Journal of Molecular Liquids 437 (2025) 128382

Contents lists available at ScienceDirect

Journal of Molecular Liquids

journal homepage: www.elsevier.com/locate/molliq

On the role of isomeric composition in determining the stability of liquid phases: A Molecular Dynamics study of acetaldehyde phenylhydrazone

Margherita Vacchini, Giovanni Macetti *, Luca Sironi, Leonardo Lo Presti *

Università degli Studi di Milano, Department of Chemistry, Via Golgi 19, 20133 Milano, Italy

ARTICLE INFO

Keywords:
Acetaldehyde phenylhydrazone
MiCMoS
Molecular dynamics
Liquid state
Chemical equilibrium

ABSTRACT

Acetaldehyde phenylhydrazone (APH) exists as a pair of E and Z isomers, but only the Z form is known to form crystals. Crystalline *Z*-APH was the subject of intense research efforts for over a century due to an erratic melting behavior, which failed to find satisfactory explanations. The mystery was solved just a few years ago, when Threlfall showed that melting involves partial isomerization, which might be sped up even by trace of acid catalysts. In this work, we apply the Molecular Dynamics tools available in the Milano Chemistry Molecular Simulation (MiCMoS) package, to explain the compositional stability range of the liquid, as estimated by NMR measurements. We also propose a cheap protocol to predict relevant thermodynamic state functions, based on experimental estimates for the equilibrium composition. We show that electrostatic interactions favor partially ordered arrangements of close neighboring molecules, which assume elongated antiparallel conformations. This interaction geometry is not easily achieved by Z isomers, which are constrained to bear partially folded hydrocarbon chains, and form liquids with lower cohesive energy. The consequence is that *E*-diluted solutions are enthalpically unfavored. Increasing the concentration of E reduces the enthalpic penalty and provides a favorable entropy of mixing, until partial molecular ordering at short range makes the entropic term unfavorable as well. The equilibrium is achieved when the entropic term is still large and positive enough to contrast the enthalpic cost. We predict that this occurs within the $0.4 \leq x_E \leq 0.6$ compositional range, in good agreement with the experimental estimate. The applicability of our method to the general case of binary mixtures of organic liquids is discussed in the context of providing a molecular-level understanding of the observed thermodynamic properties.

1. Introduction

N-(ethylideneamino) aniline, also known as acetaldehyde phenylhydrazone (APH), exists as a couple of E, Z stereoisomers (Scheme 1), depending on the relative orientation of the C-CH_3 and N—N bonds. *Z*-APH crystallizes in the monoclinic space group *Cc* (n. 9, CCDC [1] XIZKAV and XIZKAV01). No other crystal forms are known to date, and no crystals were ever reported hosting the E isomer.

APH has been largely investigated for over a century, as the same *Cc* crystal structure was found to melt sharply at different temperatures in the 56–101 °C range of T, depending on the environment and the chemical history of the specimen [2–5]. Apart coexistence with high-melting reaction byproducts [2–4,6], an obvious explanation is that different melting points could be in fact associated to barely distinguishable crystal polymorphs, which may be converted catalytically into one another under specific chemical conditions. However, this hypothesis stubbornly failed to find experimental confirmation [7–10].

The conundrum was solved only a few years ago by Threlfall and coworkers, [6] who demonstrated that the diverse melting points of APH depend on the isomeric composition of the liquid, rather than on the crystal structure. In phenylhydrazones, isomerization occurs in the liquid phase at ordinary temperatures, eventually leading to thermodynamically stable E/Z mixtures of specific compositions [11,12]. Based on NMR evidence, Threlfall et al. [6] demonstrated that molten APH at equilibrium entails both E and Z isomers in a 1.7 ratio, also in agreement with other NMR estimates [12]. Thus, they proposed that the melting point of *Cc Z*-APH ($T_m \approx 95$ °C) is lowered in the presence of weak acids (including atmospheric CO_2), due to the catalytic-aided Z-E isomerization on the crystal surface, which shifts the liquid composition toward the thermodynamically stable excess of the E form.

A point still open to investigation is the microscopic description of the liquid, *i.e.* the explanation of why the mixture of the two isomers with the Threlfall's ratio is thermodynamically favored over the liquid of pure Z. Here, we tackle the problem with classical Molecular Dynamics

* Corresponding authors.
E-mail addresses: giovanni.macetti@unimi.it (G. Macetti), leonardo.lopresti@unimi.it (L. Lo Presti).

https://doi.org/10.1016/j.molliq.2025.128382
Received 19 June 2025; Received in revised form 11 August 2025; Accepted 20 August 2025
Available online 22 August 2025

(MD) simulations of the crystal and liquid phases. We propose a cheap method to provide approximate estimates for mixing enthalpies and entropies. The method is accurate enough to predict semi-quantitatively the observed equilibrium point, which is entropy-driven and is achieved when the residual entropy of mixing is large enough to compensate for unfavorable enthalpic costs. We also show that this occurs when the favorable potential energy due to *Z*-E interactions is maximized. Implications on the general stability of liquid organic mixtures are briefly discussed.

2. Methods

2.1. Simulation of the Z-APH crystal

Molecular Dynamics (MD) simulations were carried out with the MiCMoS v2.0 and v4.0 suites of programs [13–15]. The experimental crystal structure of APH at 120(2) K was retrieved from the CSD (refcode: XIZKAV) [6] and served as a benchmark to define the Force Field parameters [15] (Section S1 in the Supporting Information, SI). A roughly cubic simulation box with edges ~33 Å long was defined, consisting of 6x2x4 repetitions of the crystallographic unit cell, for a total of 192 molecules. A 500 ps long MD simulation was carried out in *NpT* conditions with a minimal anisotropic barostat set to 1 atm with compression factor $\mu_0 = 0.35$ atm^{-1}, in conjunction with a weakly coupled Berendsen thermostat exploiting time constant $\tau = 0.6$ ps. Integration of the equations of motion was carried out using the leap-frog algorithm, with a time step of 2 fs. The Lennard-Jones-Coulomb (LJC) force field [16] gave the best agreement in terms of cell parameters and crystal density, with relative errors not exceeding ±2 %, [14] and was used throughout. Cell parameters and relevant simulated equivalent isotropic thermal parameters are deposited in Section S2 SI.

2.2. Simulation of isomerically pure APH liquids

A tentative geometry of the E isomer (Scheme 1) was generated by rigid rotation of the ethylidene substituent of Z around the imine bond. Then, both the E and Z molecules underwent quantum optimization with Gaussian16 [17] at the MP2 6-31G(p,d) level of theory *in vacuo*. The corresponding optimized geometries, complemented with CHelpG atomic charges, [18] entered the subsequent classical simulations with the LJC force field. Two approximately cubic boxes with 250 molecules each were generated with the *Boxliq* routine of MiCMoS [15] by randomizing the relative molecular positions and orientations. Hard contacts were disposed by 2.5–3·10^6 steps of Monte Carlo thermalization runs at $T = 378$ K, that is at least ~10 K above the highest reported melting temperature of *Z*-APH [6]. Both liquids underwent 1 ns long *NpT* MD equilibration runs at the same temperature, with an isotropic Berendsen barostat set to 1 atm and compressibility parameter $\mu = 0.35$ atm^{-1}, and a Berendsen thermostat with time constant of 0.6. Finally, a 4 ns long simulation using the Parrinello-Rahman barostat [19] (coupling parameter ww = 2.5 kg) and Bussi-Donadio-Parrinello CSVR thermostat [20] was performed. The same setup described above for the crystal was employed. Relevant topology and input files for liquid models are reported in Section S1 SI. Results from time-average of the last 200 ps of the equilibration run with simple rescaling algorithms are shown in Section S3 SI, while outcomes from longer production runs are reported in Sections S4 and S5 SI. Interestingly, results from 1 ns-long trajectories based on simple rescaling algorithms are mostly quantitatively identical with those obtained from 4 ns-long runs with a more sophisticated treatment of the thermodynamic boundary conditions. This indicates that the system is reasonably well-equilibrated and that the results here illustrated are robust against the details of temperature and pressure scaling, as it should be for static (not flowing) liquids in their stable thermodynamic state. If not otherwise specified, results from 4 ns-long production trajectories are discussed hereinafter.

2.3. Simulation of isomeric APH mixtures

Eight models of liquid APH mixtures at fixed compositions of E and Z isomers were developed. Relevant input files and steering parameters can be found in Section S1 SI. First, a large cubic box of 432 *E*-APH molecules was pre-equilibrated by 2.2·10^6 steps of Monte Carlo at 378 K. The same LJC Force Field was used throughout. Then, the *Solution* routine of MiCMoS [15] was employed to merge the *Z*-APH liquid box described above with the new *E*-APH one. The output was an isomeric mixture with the desired concentration of Z-APH ("solute") in E-APH ("solvent"). The E/Z ratios ranged from 0.17 (~2 M in Z-APH) to 24.14 (~0.2 M in Z-APH). The isomeric composition was kept constant during simulations by imposing a large rotation barrier (50 kJ·mol^{-1}) for the N9-N10 = C7-C8 torsion (labelled as 12–13–14-15 in the topology (.top) files, Section S1.1 SI). Values for this conformation-defining parameter did never deviate from 0° (Z) or 180° (E) by more than ±20° (see also Fig. S10 SI), indicating that no isomerization ever took place during the production runs. Preliminary MD runs at $T = 20$ K and timestep 1 fs were carried out for 0.5 ps to get rid of possible residual solute-solvent steric clashes. Then, a total of 5 ns long *NpT* trajectories evolved at 378 K and 1 atm, with the same steering parameters and strategy as described above (first ns: simple rescaling, last 4 ns: Parrinello-Rahman barostat and CSVR thermostat). To ensure that full equilibration was reached, all averages and analyses refer to the last 1 ns of each trajectory, unless otherwise indicated.

2.4. Reproducibility

The full MiCMoS package (including more recent releases) can be downloaded free of charge upon registration at https://sites.unimi.it/xtal_chem_group/, under the specified citation and use conditions. Relevant input files and topologies are available in Section S1 SI. Please refer to the available online documentation (users' manual and tutorials) for detailed procedural descriptions. The full trajectory files are available at Zenodo (doi: https://doi.org/10.5281/zenodo.15625106). This ensures complete reproducibility of the calculations here described.

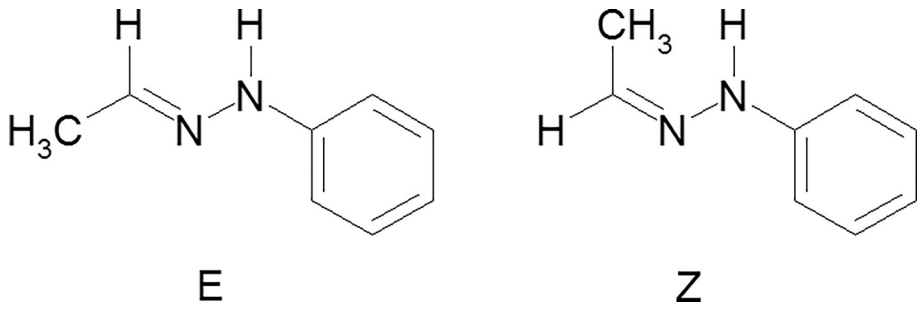

Scheme 1. Molecular connectivity of APH isomers (E and Z).

3. Results

3.1. Solid-state Z-APH

Fig. 1a shows the experimental crystal packing of Z-APH, which crystallizes in the polar *Cc* space group (n. 9). The molecular dipole moment module *in vacuo* that corresponds to the in-crystal geometry reads 2.577 D at the MP2/G-31G(p,d) level of theory and points toward the direction of the N—H donor (Fig. 1a). Both APH isomers are scarcely polar compared with compounds of similar chemical composition [21]. Moreover, as expected in the absence of strong polarization effects, [22,23] the dipole moment is almost unchanged (2.445 D) if computed on the optimized geometry *in vacuo* at the same level of theory. In the crystal, the largest dipole components lie in the (*a*,*c*) plane, determining an overall net polarization along the $[\bar{1}01]$ direction (Fig. 1a). To the sake of comparison, the *E*-APH isomer has an estimated dipole moment of 2.510 D once optimized *in vacuo* at the same level of theory. The cell dipole contribution accounts for ~14 % of the total LJC crystal cohesive energy, as estimated through the van Eijck and Kroon correction on the experimental (static) structure [24].

The crystal packing consists of linear parallel chains of *Z*-APH molecules running along the same *c* axis, held together by a 2.2 Å long NH···N head-to-tail contact that connects glide-related nearest neighbors (Fig. 1a, blue lines). Parallel chains along *b* are cross-linked by allegedly weak CH···π interactions that involve the aromatic hydrogen H2 (Fig. 1a, orange lines). The terminal methyl is hosted in the free space between adjacent molecular ribbons and does not contribute to any relevant intermolecular interaction.

The Molecular Dynamics (MD) setup (see Methods) reproduces quantitatively the packing features of *Z*-APH, as it can be appreciated by comparing the outcomes of radial distribution functions after MD equilibration (Fig. 1c,d). Correspondingly, the errors in cell edges and density are all below 2 %, in line with the expected performance of the MiCMoS force fields (see also Section S2 SI) [14,22]. As expected, [25] average atomic thermal motion amplitudes are generally underestimated with respect to the X-ray structure. However, a good linear correlation exists between experimental and predicted isotropic Debye-Waller factors, U_{eq}, of almost all the atoms of Z-APH XIZKAV (Fig. 1b). The fitting is quantitatively identical also when MD results are compared with thermal parameters of the other structure available, XIKZAV01 (Fig. S1 SI). In both cases, the patent outliers are the nitrogen atoms N9 and N10. The parametrization of the N—N group is not explicitly included in MiCMoS; thus, we cannot exclude that stretching and bending force constants related to this moiety may require finer tuning (see also Section S1 SI). Another general source of error may be the persistence of anharmonicities at 120 K, which would come unseen in

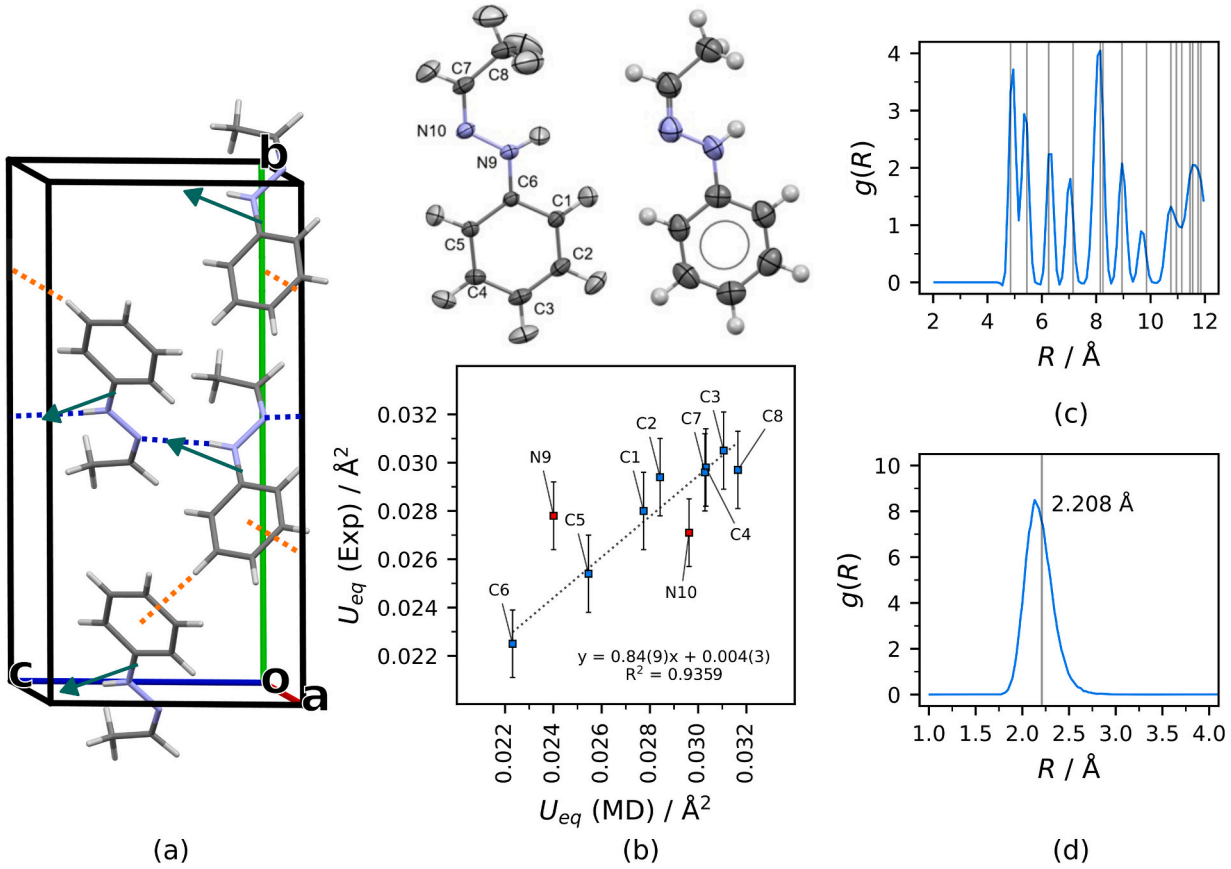

Fig. 1. Z-APH crystal at $T = 120$ K. (a): Unit cell of the experimental structure, XIZKAV, [6] seen roughly along the [101] crystallographic direction. Blue dotted line highlights NH···N hydrogen bonded contact, orange dotted line the CH···π ones. Green arrows indicate the quantum mechanical dipole moment computed at the in-crystal geometry (see text), ($|\boldsymbol{\mu}| = 2.6$ D), which forms a zig-zag motif running along the *c* axis. The tip of the arrow corresponds to the negative center of charges; the bottom end is set on the molecular center of mass. (b) Top: Asymmetric unit of *Z*-APH, with the atom numbering scheme. Thermal ellipsoids from Molecular Dynamics (MD, left) and Literature X-ray data (Expt, right) are plotted at the 80 % probability level. Bottom: linear least-squares regression between experimental and MD U_{eq} Debye-Waller parameters (Å^2). MD parameters were multiplied by a scale factor of 1.94, obtained from averaging the ratio experimental/MD parameters for all atoms. Vertical bars correspond to 2 experimental estimated standard deviation (e.s.d.); outliers are highlighted in red (see text). (c) Radial distribution function of molecular center of mass, as averaged across the last 252 frames (100.4 ps) of the MD trajectory. Vertical lines correspond to the perfect crystal structure. (d) Same as (c), for the H···N hydrogen bonded contact highlighted in (a). (For interpretation of the references to colour in this figure legend, the reader is referred to the web version of this article.)

the standard X-ray model [26–28]. However, these discrepancies did not prevent the MD model from reproducing correctly the intermolecular interaction network, and from catching the main aspects of the in-crystal conformational dynamics at least. Overall, we deem MD results accurate enough to gain insights on molecular recognition of APH.

3.2. Structure of pure liquids

Fig. 2 and Table S4 SI summarize the interaction energies of the two isomerically pure liquids. Some systematic differences can be appreciated. The cohesive energies (E_{coh}), defined as the sum of intermolecular Lennard-Jones and Coulomb contributions in the whole simulation box, are expected to correlate with vaporization enthalpies [22,29] and lie in a sharp range between −52.6 kJ·mol^{-1} (pure E) and − 46.7 kJ·mol^{-1} (pure Z).

Accordingly, the E liquid is predicted to be slightly denser than the Z one (Table S4 SI). These differences are small on absolute grounds, as their magnitude is comparable with the expected precision of MiCMoS force fields [13,14,22] and of the order of the instrumental sensitivity of calorimetric estimates for the heat of vaporization [30]. The solutions with different isomer ratio lie in between this narrow energy range. As expected, solutions rich in E are more like pure E liquid and *vice versa* (see next Section).

Differences between the pure liquids are statistically significant (~ 10 estimated standard deviations) and systematic (Fig. 2). The outcome is that the E liquid bears a slightly larger cohesion, due to Coulomb contributions that are more negative by ~5 kJ·mol^{-1} than those in Z (Table S4 SI). The reason is the slightly greater polarity of the E isomer (see above), whose ethylidene terminal chain adopts a more elongated shape (Scheme 1).

The energetic preference toward the E isomer mirrors the average structure of the liquid. Fig. 3 shows the radial distribution functions (g (r)) for molecular center of mass (C.o.M.) and H/N atoms possibly involved in hydrogen bonds. The average was carried out in the last 1 ns of the whole 4 ns-long trajectory. The g(r) curves for H···N interactions (Fig. 3b) show that the latter are significantly more frequent in the E liquid, probably due to less steric hindrance of the methyl group in E isomers [21,31]. Accordingly, the c.o.m. distributions (Fig. 3a) show similar differences, as a sharp peak at ~4.9 Å is present in the E liquid but is absent in the Z one. This feature is due to stacking approaching modes, where adjacent molecules align their main axes along the imine

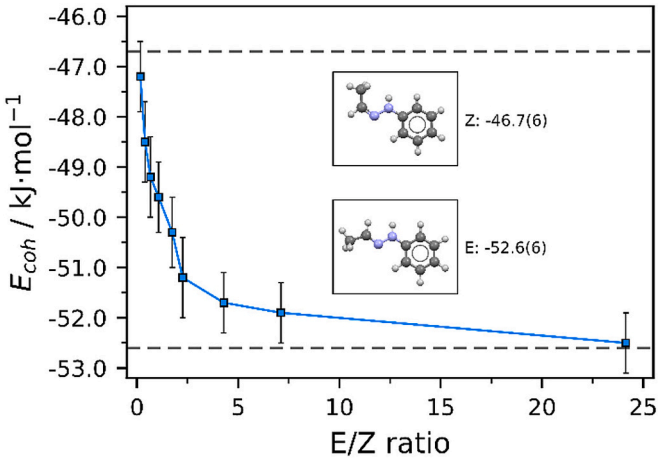

Fig. 2. Cohesive energy (kJ·mol^{-1} per molecule), defined as the sum of Lennard-Jones and electrostatic contributions for APH liquid solutions, as a function of the E/Z ratio. The horizontal lines refer to isomerically pure E and Z limits (E/Z = ∞, E/Z = 0). Vertical bars and number in parentheses represent 1 estimated standard deviation (e.s.d.) from MD averaging over the last ns of the 4 ns-long MD trajectory. The corresponding numerical entries can be found in Tables S4 and S6 SI.

chain in an antiparallel fashion to maximize direct dipole-dipole interactions. Occasional favorable π···π geometries may provide extra stabilizing contributions (Fig. 3a). Despite being present in both liquids, this kind of interaction geometry is statistically more frequent in E and results, on average, in closer (and greater cohesion) of E molecules. This occurs at the expense of the broad peak at ~6.9–7.0 Å, which accordingly is significantly more populated in the Z liquid. This feature is mainly due to molecules that sit side by side roughly in the same plane (Fig. 3a, right) or approach each other perpendicularly in a "T" fashion (Fig. S9 SI).

It is worth noting that the $g(r)$ features above discussed are already appreciable after the first 1 ns of equilibration under simple rescaling algorithms (Fig. S2 SI). Thus, they should be correlated with true structural differences between the equilibrated liquids, as they are simulated at high temperature above their melting point, where thermal fluctuations are expected to occur with very fast kinetics [32]. Interestingly, if centroids of aromatic rings are employed as reference points for $g(r)$ instead of C.o.M.'s (Section 4.1 SI, Fig. S13), two intense and almost identical peaks are appreciable at ≈ 5.8 (E) and ≈ 6.0 (Z) Å. These quite large and similar distances indicate that, on average, aromatic rings of adjacent molecules interact weakly with each other, implying that stacking interactions are expected to be poorly relevant in determining the structure of either of the two liquids. In turn, these structural differences may be traced back to the different shape of E and Z isomers. The C═N double bond forces the terminal methyl to fold back toward the aromatic ring in Z, while in E the hydrocarbon chain can afford a more linear configuration. The consequence is a more compact shape of Z, which hampers the possible beneficial effects of dipole-dipole coupling. This hypothesis is substantiated by the comparison of intramolecular torsion energies, which are greater in the Z isomer by +2.3(7) kJ·mol^{-1} per molecule when averaged over the last 1 ns of the trajectory, while stretching and bending contributions of Z and E are identical (Table S4 SI).

This implies that the intermolecular potential produces slightly larger average conformational distortions in Z molecules. This is likely due to steric hindrance of the *cis* methyl, which is forced to lie close to the aromatic ring due to the orientation of substituents around the double bond (red bars in Fig. S10 SI, Table S5 SI). Distorted conformations where the hydrocarbon chain is no longer parallel to the aromatic plane alleviate the Pauli repulsion.

In conclusion, we hypothesize that the folded configuration of the Z isomer hampers favorable dipolar interactions with next neighbors, as it slightly lowers the overall dipole moment and, at the same time, makes the setup of elongated molecular conformations less frequent. This is consistent to the lower density of the liquid of Z at equilibrium, as well as to the significantly lower frequency of stacking contacts below 5 Å.

3.3. Thermodynamics of the solutions

Figs. 4a,b show the thermodynamic state functions associated to the isomerization process, as estimated from Literature experimental data [6,12] complemented by our MD simulations according to eqs. (1–5) below. At the melting point, liquid *Z*-APH transforms into *E*-APH according to the monomolecular isomerization equation:

$$Z \rightleftarrows E \tag{1}$$

The free energy of reaction is

$$\Delta_R G = \Delta_R G^o + RT\ln\left(\frac{[E]}{[Z]}\right) \tag{2}$$

In (2), $\Delta_R G^o$ is the standard Gibbs free energy at 1 bar, T is the temperature (378 K) and R = 8.314 J·K^{-1}·mol^{-1} is the gas constant. It is easy to see that the reaction quotient $[E]/[Z]$ is equal to the E/Z ratio, which was kept fixed during each MD simulation (see Methods). We assume that the experimental Threlfall's NMR estimate [6] of 1.7 for the

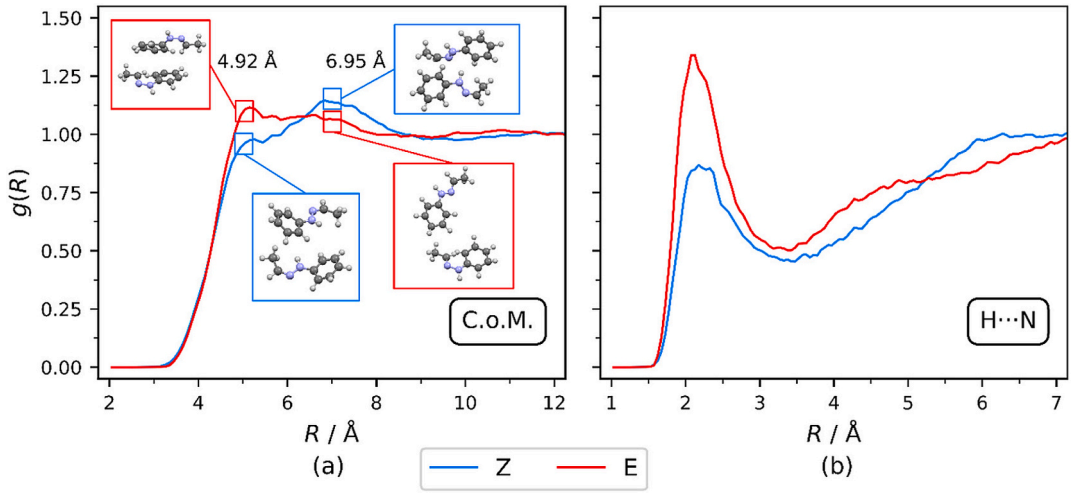

Fig. 3. (a) Radial distribution function, $g(r)$, for molecular center of mass (c.o.m.) of Z (blue) and E (red) isomers of liquid APH at 378 K, as averaged from the last 1 ns of the 5 ns-long trajectory. Inset: examples of interaction geometries for close molecular pairs at ~4.9 and ~ 6.9 Å, taken from the last frame of the trajectory. See Fig. S9 SI for more examples. (b) Same as (a), for N9–H···N10 (Scheme 1). As the number of molecules is the same in both models for the E and Z liquid (see Methods), all the functions in this Figure are plotted on the same scale. Fig. S13 SI shows the same results, using center of coordinates of the phenyl group as the reference point. (For interpretation of the references to colour in this figure legend, the reader is referred to the web version of this article.)

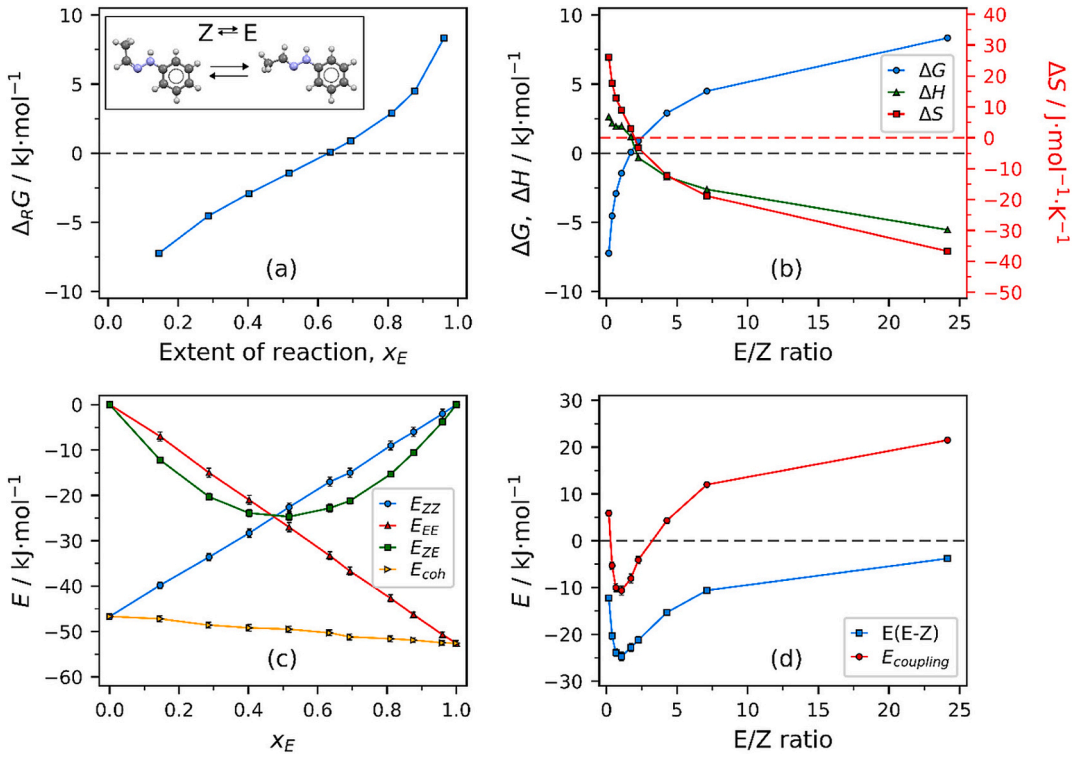

Fig. 4. (a) Gibbs energy (kJ·mol^{-1}) of isomerization computed for different extent of the $Z \rightleftarrows E$ reaction, assuming E/Z = 1.7 as equilibrium composition (see text). The horizontal black line marks the equilibrium point. (b) Same as (a), plotted against the E/Z ratio. Also, isothermal-isobaric enthalpic (kJ·mol^{-1}) and entropic contributions are given. Entropy is plotted with respect to the secondary axis on the right (red) in J·K^{-1}·mol^{-1}. The horizontal lines give the 0 entropy (red) and free energy (black) references. (c) Contributions to the cohesive energy for *Z*-Z, E-E and E-Z molecular pairs as a function of mole fraction of E (x_E). (d) Z-E interaction energy, E_{EZ}, and coupling energy, E_{coup} (see text) as a function of the E/Z ratio. The horizontal bar marks zero energy (no *E*-Z interaction at all). In all plots, lines are only guides for the eye. The corresponding numerical entries can be found in Tables S6-S7 SI. (For interpretation of the references to colour in this figure legend, the reader is referred to the web version of this article.)

equilibrium isomeric composition at $T = 105$ °C is correct – which is reasonable also from a molecular point of view, as it is demonstrated below. Thus, $\Delta_R G = 0$ for $\frac{[E]}{[Z]} = 1.7$, resulting in $\Delta_R G^o = -1.668$ kJ·mol^{-1}. From (2), $\Delta_R G$ can be predicted at any simulated composition (Fig. 4a). This quantity is the slope of G against the extent of reaction, which here is exactly the mole fraction of the E isomer (x_E), and is equal to the difference of chemical potential of E and Z for that composition:

$$\Delta_R G = \left(\frac{\partial G}{\partial x_E}\right)_{p,T} = \mu_E - \mu_Z \tag{3}$$

As expected, the imbalance of chemical potential is roughly symmetrical. It assumes highest values, up to ±8 kJ·mol^{-1}, at extreme dilutions of either E or Z and approaches zero linearly at intermediate compositions. Fig. 4b shows enthalpy ($\Delta_R H$) and entropy ($\Delta_R S$) contributions for (1) as a function of the E/Z ratio. $\Delta_R H$ can be estimated from MD simulations according to:

$$\Delta_R H = E_{coh,EZ} \bullet N\left(\frac{E}{Z}\right) - E_{coh,Z} \bullet N(Z) + p \bullet \Delta V \quad (4)$$

In (4), $E_{coh,EZ}$ is the average cohesive energy for the mixture with a given E/Z ratio, and $E_{coh,Z}$ is the same quantity for the isomerically pure Z liquid. Both energies are expressed in kJ·mol^{-1} per molecule; thus, they must be multiplied by the corresponding number of molecules, $N(E/Z)$ and $N(Z)$, to obtain the correct estimate in kJ·mol^{-1} for the whole simulation box. The Legendre term $p{\cdot}\Delta V$ accounts for the expansion work due to the change of the simulation box volume upon going from pure Z to any E/Z solution. The term $p{\cdot}\Delta V$ is very small, as it ranges between ±1.3 kJ·mol^{-1} throughout the whole compositional range. It is negative for *Z*-rich solutions and positive for *E*-rich ones, with 0 occurring at E/Z = 4.29 (0.7 M). $\Delta_R H$ expresses the amount of heat that the system exchanges at constant pressure when some Z molecules of the isomerically pure liquid are changed into an equimolar amount of E to produce a solution at the desired E/Z composition. Finally, as the MD simulations were carried out in isothermal isobaric conditions, identity (5) holds:

$$\Delta_R S = \frac{\Delta_R H - \Delta_R G}{T} \quad (5)$$

The initial addition of E to pure Z is endothermic by ~4 kJ·mol^{-1} but mixing becomes quickly exothermic over E/Z = 2 (green curve in Fig. 4b). This mirrors the setup of more favorable *E*-E interactions (see above), which require that concentration be large enough to be effective.

In contrast, high concentrations of E imply unfavorable entropic contributions (Fig. 4b, red curve), which can be explained with the loss of degrees of freedom due to favorable dipole-dipole and stacking interactions at short range (Fig. 3a). At E/Z = 1.74, very close to the experimental equilibrium point, $\Delta_R S$ provides a favorable contribution that contrasts the endothermic energy expense.

More insights can be obtained by dissecting the molecular cohesive energy into contributions from E and Z (Fig. 4c,d). In MiCMoS [15] interaction energies are computed in a pairwise atom-atom fashion. This approach allows the exact partitioning of the total cohesive energy (E_{coh}, kJ·mol^{-1} per molecule) according to

$$E_{coh} = E_{ZZ} \bullet x_Z + E_{EE} \bullet x_E + E_{EZ} \quad (6)$$

In (6), E_{ZZ}, E_{EE} and E_{EZ} are the normalized interaction energies per molecule that involve species *Z*-Z, *E*-E and E-Z, while x_Z and x_E are the corresponding mole fractions. These energies are directly related to the corresponding vaporization enthalpies, [13,15,22,33] that is, to the strength of intermolecular interactions in the liquid. It turns out (Fig. 4c) that the E_{EZ} cross term is always lower in magnitude (less negative) than the corresponding E_{ZZ}, E_{EE} ones in pure liquids, indicating that interactions between E and Z are weaker, on average, than those of each isomer by itself. In other words, at low concentrations E ruffles the short-range structure of Z but it is too diluted to set up favorable interactions with other E molecules. The net outcome is an unfavorable (endothermic) enthalpic cost (Fig. 4b). Note, however, that this does not mean that E-Z interactions are unfavorable or negligible in some way. Rather, they account for up to 47–49 % of total E_{coh} (Fig. 4c, Table S6 SI). The most negative E_{EZ} contribution occurs close to $x_E \approx 0.5$, as would be expected for components with high chemical similarity. A change of coordinate (Fig. 4d) shows indeed that E_{EZ} has a sharp minimum in a restricted E/Z range around 1.0–2.0. Energies corresponding to E/Z ≈ 0.7, 1.0 and 1.7 are identical within 1 estimated standard deviation (Fig. 4d and Table S6 SI), which compares well with Threlfall's NMR estimate (1.7) [6]. The main take-home message is that the experimental isomeric ratio corresponds to a rather narrow compositional range ($0.4 \le x_E \le 0.6$ or $0.7 \le E/Z \le 1.7$) where the interaction energy between the E and Z achieves the most negative values.

In analogy to what has been done for crystalline binary mixtures, [34] it may be convenient to define a "coupling energy", E_{coup}, according to (7):

$$E_{coup} = E_{EZ} - \frac{1}{2}(E_{ZZ} \bullet x_Z + E_{EE} \bullet x_E) \quad (7)$$

All interaction energies being negative numbers, $E_{coup} < 0$ implies that stabilizing contributions due to cross-interactions overcome the average contributions from individual components of the mixture. On the contrary, whenever $E_{coup} > 0$, the opposite is true, *i.e.* E and Z, on average, set up more favorable interactions with themselves rather than with each other. It is easy to see (Fig. 4d) that this is always true at extreme dilutions of either component. Thus, E_{coup} could be approximately correlated to the thermodynamic drive toward the formation of a stable solution and determines the corresponding favorable compositional range. From Fig. 4d it is clear that E_{coup} strongly correlates with E_{EZ}. Thus, it is reasonable to assume that the most probable composition according to MD outcomes is that corresponding to the minimum of the E_{coup} function. This occurs at E/Z ≈ 1.1, even though the neighboring points of both E_{coup} and E_{EZ} are identical within 1 estimated standard deviation. Considering the classical nature of our force-field based simulations, as well as the unavoidable errors due to neglecting multibody contributions, it can be concluded that there is a fair qualitative conformity of views with the experimental outcome. Moreover, both the isomerization enthalpy (Eq. 4) and the coupling energy (Eq. 7) below are derived from energy differences at equilibrium. As a result, these quantities tend to remain relatively robust against any adjustment of the force field. If E/Z = 1.1 is taken as the best MiCMoS prediction, the relative error amounts to −18 %, as MiCMoS downshifts the absolute minimum of E_{EZ} at $x_E = 0.517$, while NMR estimates indicate $x_E = 0.629$ as the most likely composition [6,12]. The present MD simulations strongly suggest that the actual compositional stability range of the liquid may not be necessarily restricted to the ratio E/Z = 1.7 only.

Fig. 5 ab shows the Lennard-Jones and Coulomb contributions to total Z-Z, *E*-E and E-Z energies, as a function of the E/Z ratio. Two points are worth noting. First, the dispersive interactions are up to three times more negative than the electrostatic ones. Second, the Coulomb term follows the same trend as the LJ one. In both cases, *Z*-Z and E-E contributions achieve their extreme values at extreme compositions, while E-Z has a sharp minimum in the same compositional range as the total E-Z energy (Fig. 4d). As the isotropic Lennard-Jones potential dominates, in analogy also to other organic liquids, [35] the cohesion is not due to directional molecule-molecule contacts. This is confirmed by Fig. 5c, where the radial distribution function of Z-Z, *E*-E and E-Z molecular center of mass, $g(r)$, is shown for E/Z = 1.74, which is closest to the experimental equilibrium composition. Proximity of E and Z species is slightly more frequent than Z-Z at $r \approx 5$ Å, as E is the majority isomer in this solution. However, no clear evidence is given on the setup of a permanent solvation shell involving close E-Z neighbors. The frequency of hydrogen bonds as a function of the E/Z ratio is quite low, between 0.05 and 0.25 bonds per frame per molecule across the whole range of composition (Fig. 5d). Solutions richer in the E have a greater average number of hydrogen bonds, owing to the lower availability of the NH group as a donor in the Z isomer due to the steric hindrance of the terminal methyl (see Fig. 3b above and discussion therein). Considering *E*-Z cross contacts, the frequency of hydrogen bonds has maximum at E/Z ≈ 1 and correlates with Z-E interaction energy, coupling energy (Fig. 4d) and both electrostatic and dispersive terms (Figs. 5a,b). Even though it certainly provides some cohesive terms, it is improbable that such a low hydrogen bond frequency plays a major role in explaining the enhanced stability of solutions in this range of concentrations. Most likely, this increase in the E-Z hydrogen bond frequency (Fig. 5d, green line) is due

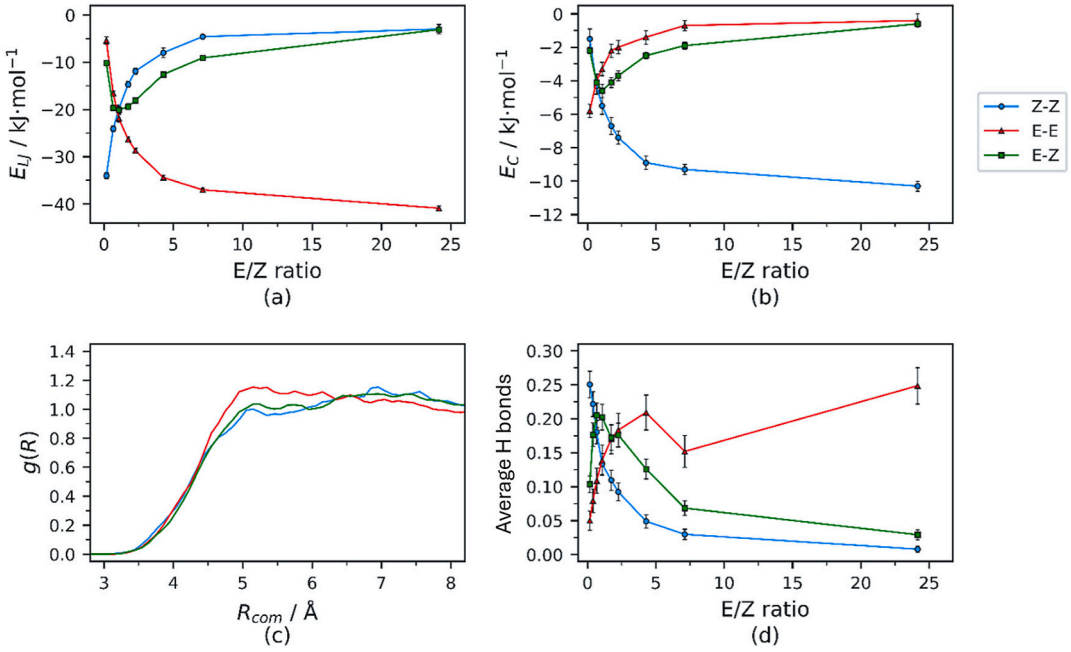

Fig. 5. (a-b) Dissection of *Z*-Z (blue), *E*-E (red) and E-Z (green) Lennard-Jones (E_{LJ}) and Coulomb (E_C) energy contributions, in kJ·mol^{-1} per molecule, as a function of chemical composition of APH solutions. The corresponding numerical data are shown in Table S8 SI. (c) Center of mass (C.o.M.) radial distribution function for E/Z = 1.74. The *E*-E curve is slightly higher than the *Z*-Z one around 5 Å as E is the majority isomer in this solution. See Figs. S11-S12 SI for plots corresponding to other compositions, and Figs. S14-S15 SI for $g(r)$'s referred to the geometrical center of the phenyl moiety. (d) Number of hydrogen bonds per frame per molecules, as averaged for the last 1 ns of trajectory.

to more favorable electrostatic interactions, which provide a drive toward more favorable interaction geometries.

We expect that the above discussed results are reasonably accurate, as addition to extra energy terms to account for interactions that are neglected by the LJC force field, like multi-body and polarization contributions, will provide only small corrections to total cohesive energy. In fact, the LJC force field was parametrized to reproduce satisfactorily the vaporization enthalpies of >300 organic liquids [16]. Any more accurate parametrization specific for APH solutions would require the availability of as much accurate experimental estimates of mixing enthalpies.

In conclusion, directional favorable dipolar interactions favor the alignment of close neighboring molecules, which in turn favors elongated conformation (see previous Section) and maximizes the number of atom-atom close contacts. The net outcome is the enhancement of attractive dispersive *E*-Z terms (Fig. 5a). However, Z isomers cannot achieve a fully elongated conformation due to intrinsic folding of their terminal methyl group (see above). Thus, the addition of E produces a configurational mismatch, which makes $\Delta_R H$ slightly positive (Fig. 4b). At the same time, the partial ordering due to electrostatics is insufficient to compensate for the $\Delta_R S > 0$ mixing term (Fig. 4b). Overall, this entropic term balances unfavorable enthalpic one, and the system is at (or close to) equilibrium at this concentration.

4. Conclusions

The elusive melting behavior of acetaldehyde phenylhydrazone (APH) remained an unsolved conundrum for a long time. Only recently, Threlfall and co-workers discovered that the explanation resides in the E-Z isomeric structure of the melt, whose stable composition corresponds to a ratio of E/Z = 1.7. As the solid contains only Z species, isomerization must occur at the solid-liquid equilibrium boundary. Acid catalysts could speed up the process, lowering the apparent melting point of the crystal.

In this work, we provide a possible microscopic explanation of the observed isomeric stability of APH liquids. By means of classical Molecular Dynamics (MD) calculations, we simulate APH solutions at different isomeric compositions, and we provide estimates of the corresponding thermodynamic state functions by first performing an equilibration run of 1 ns with simple rescaling algorithms and then extending the dynamic up to 5 ns using more the sophisticated CSVR and Parrinello-Rahman procedures. The results are almost unchanged (Sections S3 and S4 SI), which implies that the equilibrium properties extracted from our trajectory likely refer to true equilibrium states and are robust against the details of the computational setup. We show that the cohesion of the melt is driven by dispersive interactions. However, electrostatics favors partially ordered arrangements of close neighboring molecules, which tend to assume elongated conformations that allow the antiparallel alignment of their hydrocarbon chains. Isomers in "E" configuration are prone to achieve this setup, as no steric constraints prevent them from unfolding. However, the same favorable interactions have a significant entropic cost, which may amount up to −37 J·K^{-1}·mol^{-1} for liquids very rich in E. At the same time, solutions diluted in E are enthalpically unfavored, due to the lower intrinsic cohesion of the Z liquid itself. The equilibrium is genuinely entropy-driven, and it is achieved when the residual entropy of mixing is still positive and large enough to compensate for the enthalpic cost. Interestingly, this occurs when the potential energy of interaction between the E and Z isomers overwhelms that of both *E*-E and *Z*-Z pairs, as it can be quantified by means of coupling energies.

Notably, the approach here presented is not restricted to the title compound but has general applicability for any binary mixture of organic liquids. We propose an inexpensive method to extract sensible thermodynamic state functions from MD simulations, which is based on the knowledge of the correct equilibrium point from reliable experimental sources. As for the title compound, the conformity of views between experimental NMR estimates and our Force Field-based approach is semi-quantitative and may help to delve into deeper insights into structure and properties of complex liquids, which are not within the reach of experimental methods. The idea is to highlight how conformational and configurational degrees of freedom are intertwined in solutions, with the broader goal of designing organic liquids with the

desired properties. These aspects require more in-depth investigation and will be the subject of forthcoming studies.

A limitation of this approach is that it does not allow us to delve into kinetics of isomerization, as our simulations are based on liquids at equilibrium and the force field does not allow E-Z interconversion. Data obtained from NMR experiments could be highly informative providing, for example, experimental estimates of the energy barriers involved to allow a detailed characterization of the isomerization kinetics of APH. This topic will be possibly dissected in further studies.

Ethical concerns

Not applicable to this work.

CRediT authorship contribution statement

Margherita Vacchini: Writing – review & editing, Investigation, Formal analysis. **Giovanni Macetti:** Writing – review & editing, Software, Formal analysis. **Luca Sironi:** Writing – review & editing, Software, Formal analysis. **Leonardo Lo Presti:** Writing – original draft, Supervision, Resources, Data curation, Conceptualization.

Declaration of competing interest

The authors declare that they have no known competing financial interests or personal relationships that could have appeared to influence the work reported in this paper.

Acknowledgements

Thanks are due to prof. Angelo Gavezzotti for continuous encouragement and inspiration. Università degli Studi di Milano is also acknowledged for funding this research through the program “Piano di sostegno alla ricerca 2023-2024” (grant number PSR2023_DIP_005_PI_LLOPR). This paper is made available in Open Access through the CRUI-CARE agreement funded by the Italian Ministry of University and Research (MUR).

Appendix A. Supporting Information Available

Input and procedures for Molecular Dynamics. MD outcomes: crystal. MD equilibration results for liquids with simple rescaling algorithms. MD outcomes from 4 ns-long production runs: liquids. Equilibration. Supplementary data to this article can be found online at [https://doi.org/10.1016/j.molliq.2025.128382].

Appendix B. Supplementary data

Supplementary data to this article can be found online at https://doi.org/10.1016/j.molliq.2025.128382.

Data availability

All the necessary information to access data on which this Manuscript relies are reported in the main text, Methods Section, 2.4 Reproducibility paragraph

References

[1] C.R. Groom, I.J. Bruno, M.P. Lightfoot, S.C. Ward, The Cambridge structural database, Acta Crystallogr. 72 (2016) 171–179, https://doi.org/10.1107/S2052520616003954.
[2] E. Fischer, Ueber die Phenylhydrazone der Aldehyde, Ber. Dtsch. Chem. Ges. 30 (1897) 1240–1243.
[3] E. Fischer, Ueber das Azophenyläthyl und das Acetaldehydphenylhydrazon, Ber. Dtsch. Chem. Ges. 29 (1896) 793–797.
[4] M.H. Causse, Sur les aldéhydates de phénylhydrazine, Compt. Rend. 122 (1896) 1274–1277.
[5] M.H. Causse, Sur l’action de l’aldéhyde éthylique sur la phénylhydrazine et sur deux triéthylidènes-diphénylhydrazones isomériques α et β, Bull. Soc. Chim. Fr. 17 (1897) 234249.
[6] C. Bernades, M. Carravetta, S.J. Coles, E.R.H. van Eck, H. Meekes, M.E.M. da Piedade, M.B. Pitak, M. Podmore, T.A.H. de Ruiter, L.-C. Söğütoğlu, R.R. E. Steendam, T. Threlfall, The curious case of acetaldehyde Phenylhydrazone: resolution of a 120 year old puzzle where forms with vastly different melting points have the same structure, Cryst. Growth Des. 19 (2019) 907–917, https://doi.org/10.1021/acs.cgd.8b01459.
[7] E. Bamberger, W. Pemsel, Zur Kenntniss des Acetaldehydphenylhydrazons, Zur Kenntniss Des Acetaldehydphenylhydrazons, Ber. Dtsch. Chem. Ges. 36 (1903) 85–89.
[8] G. Lockemann, O. Liesche, Zur Kenntniss des Aethylidenphenylhydrazins. Justus Liebigs Ann, Justus Liebigs Ann. Chem. 342 (1905) 14–50.
[9] W. Robertson, Solubility as a measure of the change undergone by isodynamic hydrazones: (1) camphorquinonephenylhydrazone, (2) acetaldehydephenylhydrazone, J. Chem. Soc. Trans. 87 (1905) 1298–1302.
[10] E. Laws, N.V. Sidgwick, Isomeric acetaldehydephenylhydrazones, J. Chem. Soc. Trans. 99 (1911) 2085–2093.
[11] A.J. Bellamy, J. Hunter, EZ-isomerism in alkyl phenyl ketone phenylhydrazones and acetaldehyde phenylhydrazone, J Chem Soc Perkin 1 (1976) 456, https://doi.org/10.1039/p19760000456.
[12] G.J. Karabatsos, R.A. Taller, Structural studies by nuclear magnetic resonance, V. Phenylhydrazones, J. Am. Chem. Soc. 85 (1963) 3624–3629.
[13] A. Gavezzotti, L. Lo Presti, S. Rizzato, Molecular dynamics simulation of organic materials: structure, potentials and the MiCMoS computer platform, CrystEngComm 24 (2022) 922–930, https://doi.org/10.1039/d1ce01360b.
[14] A. Gavezzotti, L. Lo Presti, Molecular dynamics simulation of organic crystals: introducing the CLP-dyncry environment, J. Appl. Crystallogr. 52 (2019) 1253–1263, https://doi.org/10.1107/S1600576719012238.
[15] L. Lo Presti, A. Gavezzotti, MiCMoS v2.0 User’s Manual. See. https://sites.unimi.it/xtal_chem_group/, 2021.
[16] A. Gavezzotti, L. Lo Presti, S. Rizzato, Mining the Cambridge database for theoretical chemistry. Mi-LJC: a new set of Lennard-Jones–coulomb atom–atom potentials for the computer simulation of organic condensed matter, CrystEngComm 22 (2020) 7350–7360, https://doi.org/10.1039/D0CE00334D.
[17] M.J. Frisch, et al., Gaussian16 revision A.03, Gaussian Inc., 2016.
[18] C.M. Breneman, K.B. Wiberg, Determining atom-centered monopoles from molecular electrostatic potentials - the need for high sampling density in formamide conformational-analysis, J. Comput. Chem. 11 (1990) 361–373.
[19] M. Parrinello, A. Rahman, Crystal structure and pair potentials: A molecular-dynamics study, Phys. Rev. Lett. 45 (1980) 1196–1199, https://doi.org/10.1103/PhysRevLett.45.1196.
[20] G. Bussi, D. Donadio, M. Parrinello, Canonical sampling through velocity rescaling, J. Chem. Phys. 126 (2007) 014101, https://doi.org/10.1063/1.2408420.
[21] G. Macetti, L. Sironi, C. Rovida, I. Geremia, R. Soave, L. Lo Presti, On the solubility of azodicarbonamide in water/DMSO mixtures: an experimental and computational study, R. Soc. Open Sci. 11 (2024).
[22] M.A. Spackman, P. Munshi, B. Dittrich, Dipole moment enhancement in molecular crystals from X-ray diffraction data, ChemPhysChem 8 (2007) 2051–2063.
[23] L. Lo Presti, A.M. Orlando, L. Loconte, R. Destro, E. Ortoleva, R. Soave, C. Gatti, Single N-C bond becomes shorter than a formally double N=C bond in a thiazete-1,1-dioxide crystal: an experimental and theoretical study of strong crystal field effects, Cryst. Growth Des. 14 (2014) 4418–4429, https://doi.org/10.1021/cg500518a.
[24] B.P. van Eijck, J. Kroon, Coulomb energy of polar crystals, J. Phys. Chem. B101 (1997) 1096–1100, https://doi.org/10.1021/jp962785u.
[25] A. Nemkevich, H.-B. Bürgi, M.A. Spackman, B. Corry, Molecular dynamics simulations of structure and dynamics of organic molecular crystals, Phys. Chem. Chem. Phys. 12 (2010) 14916, https://doi.org/10.1039/c0cp01409e.
[26] R. Destro, P. Roversi, M. Barzaghi, L. Lo Presti, Anharmonic thermal motion modelling in the experimental XRD charge density determination of 1-Methyluracil at T = 23 K, Molecules 26 (2021) 3075, https://doi.org/10.3390/molecules26113075.
[27] R. Herbst-Irmer, D. Stalke, Experimental charge-density studies: data reduction and model quality: the more the better? Acta Crystallogr. Sect. B: Struct. Sci. Cryst. Eng. Mater. 73 (2017) 531–543, https://doi.org/10.1107/S2052520617007016.
[28] M. Lutz, T.J. Smak, A.T. Sanderse, Anharmonic motion in the crystal structure of 2-Mercaptopyridone, Crystals (Basel) 12 (2022).
[29] J.S. Chickos, A. Gavezzotti, Sublimation enthalpies of organic compounds: A very large database with a match to crystal structure determinations and a comparison with lattice energies, Cryst. Growth Des. 19 (2019) 6566–6576.
[30] N.S. Osborne, D.C. Ginnings, Measurements of heat of vaporization and heat capacity of a number of hydrocarbons, J. Res. Natl. Bur. Stand. 39 (1947) 453–477.
[31] L. Lo Presti, On the significance of weak hydrogen bonds in crystal packing: a large databank comparison of polymorphic structures, CrystEngComm 20 (2018) 5976–5989, https://doi.org/10.1039/C8CE00674A.
[32] L. Sironi, G. Macetti, L. Lo Presti, Nanoscale inhomogeneities in undercooled benzoic acid: A molecular dynamics study, J. Mol. Liq. 414 (2024) 126141, https://doi.org/10.1016/j.molliq.2024.126141.
[33] A. Gavezzotti, Molecular Aggregation. Structure Analysis and Molecular Simulation of Crystals and Liquids. IUCr Monographs on Crystallography n. 19, on

behalf of International Union of Crystallography, Oxford University Press, New York, 2007. ISBNs: 019857085, 9780198570806.
[34] A. Gavezzotti, V. Colombo, L. Lo Presti, Facts and factors in the formation and stability of binary crystals, Crystal Growth Des 16 (2016) 6095–6104.
[35] A. Gavezzotti, L. Lo Presti, A theoretical study of chiral carboxylic acids. Structural and energetic aspects of crystalline and liquid states, Cryst. Growth Des. 5 (2015) 3792–3803.